九州大学大学院総合理工学府報告
第 41 巻 第 2 号 22-29 頁 令和 2 年 2 月

Engineering Sciences Reports, Kyushu University
Vol. 41, No. 2, pp. 22-29, FEB, 2020

Hydrogen Production from Formic Acid Decomposition Using Au@Pd and Au@Pd/TiO_2 Core–shell Nanocatalysts Prepared by Microwave Heating

Masaharu TSUJI[*1,2†] Kento FUKUTOMI[*3] Masashi HATTORI[*1] Daisuke SHIMAMOTO[*3] Keiko UTO[*1] Jun-Ichiro HAYASHI[*1,2] and Takeshi TSUJI[*4]
[†]E-mail of corresponding author: tsuji@cm.kyushu-u.ac.jp

(Received January 23, 2020, accepted January 30, 2020)

Formic acid (FA: HCOOH) has attracted attention as a liquid fuel for use in hydrogen fuel cells because it has high energy density and it can be handled safely. For hydrogen production from FA decomposition at low temperature, Au@Pd core–shell nanocatalysts supported on TiO_2 nanoparticles were prepared using microwave (MW) heating. The hydrogen production rates, 0.13, 0.21, and 3.2 L g^{-1} h^{-1}, were obtained using Au@Pd/TiO_2 at 30, 60, and 90 °C, respectively. These values were larger than those obtained for bare Au@Pd catalysts by factors of 3.0, 1,8, and 1.5, respectively. Based on negative chemical shifts of Pd peaks found in XPS data of Au@Pd/TiO_2 particles in comparison with those of bare Au@Pd ones, the enhancement of catalytic activity of Au@Pd particles in the presence of TiO_2 was explained by an electron-donating effect of TiO_2 to Pd shells. This effect enhances the adsorption of formate to catalyst and dehydrogenation from formate leading to H_2 + CO_2.

Key words: *Hydrogen production, Formic acid, Au@Pd core–shell nanocatalyst, TiO_2 support, Microwave heating*

1. Introduction

Hydrogen is a promising energy carrier that can be used to generate electricity in a fuel cell with water being the only waste product. The search for effective techniques of hydrogen gas generation from liquid fuels has remained a difficult challenge for mobile hydrogen energy systems. In this respect, formic acid (FA) attracts great attention as a liquid fuel because it has high energy density, nontoxicity, and excellent stability at room temperature. It is known that Pd-based catalysts involving core–shell and alloy types of catalysts are effective for the production of hydrogen from the decomposition of FA at room temperature.[1-8] According to a systematic study on M@Pd (M = Ru, Rh, Pt, Ag, Au) core–shell nanocatalysts for the production of hydrogen from the decomposition of FA,[9] which gave higher catalytic activity than pure Pd/C catalysts, the best catalytic activity has been obtained from Ag@Pd catalysts, for which a high initial hydrogen rate of about 4 L g^{-1} h^{-1} was achieved at room temperature. The highest catalytic activity of Ag@Pd core–shell nanocatalysts was explained by the largest electron transfer from the Ag core to the Pd shell because of the lowest work function of Ag (4.7 eV) among M compared with that of Pd (5.1 eV).

To enhance the catalytic activity, we have recently studied the preparation of Ag@Pd nanocatalysts loaded on TiO_2 nanoparticles using a microwave (MW) heating in ethylene glycol (EG) and aqueous solution,[10-13] wherein EG and polyvinylpyrrolidone (PVP) were used as reductants.[14,15] An advantage of MW heating in comparison with conventional oil-bath heating is strong adhesion of Ag@Pd catalysts on TiO_2 support. Based on spherical-aberration-corrected scanning transmission electron microscopy (Cs-corrected STEM), STEM-energy dispersed X-ray spectroscopy (EDS), X-ray diffraction (XRD), and X-ray photoelectron spectroscopy (XPS), it could be noted that the product nanocatalysts consisted

*1 Institute for Materials Chemistry and Engineering, and Research and Education Center of Green Technology
*2 Department of Applied Science for Electronics and Materials
*3 Department of Applied Science for Electronics and Materials, Graduate Student
*4 Department of Materials Science, Shimane University

of an Ag–Pd alloy core and Pd shell nanocrystals loaded on anatase type TiO_2 nanoparticles. Ag and Pd atoms were partially alloyed with each other under MW heating in EG or H_2O. Therefore, $Ag_{93}Pd_7$ alloy core and Pd shell catalysts were formed in H_2O solution even at a short irradiation time (30 min). Using a TiO_2 support, about 13 times higher hydrogen production rate of 46.03±2.2 L g^{-1} h^{-1} at 30 °C was obtained than that attained without a TiO_2 support (3.67 L g^{-1} h^{-1} at 20 °C).[9] The significant enhancement of catalytic activity of $Ag_{93}Pd_7$@Pd in the presence of TiO_2 was explained by further electron transfer from TiO_2 to Pd because the work function of TiO_2 (4.0 eV) is lower than that of Ag (4.7 eV) and Pd (5.1 eV).

In this study, FA decomposition was studied using bare Au@Pd and Au@Pd/TiO_2 catalysts to examine the effects of core-metal M and the presence of TiO_2 support in the M@Pd catalysts. Catalytic activity was examined at 30, 60, and 90 °C to determine activation energies of Au@Pd and Au@Pd/TiO_2 catalysts for FA decomposition. The results obtained are compared with those of AgPd@Pd and AgPd@Pd/TiO_2 catalysts reported previously.[10-13]

2. Experimental

2.1. Materials

$HAuCl_4{\cdot}4H_2O$ (>99.0%), sodium citrate ($Na_3C_6H_5O_7{\cdot}2H_2O$), ethanol (>99.5%), and PVP (average molecular weight of 10 k in terms of monomer units) were obtained from Kishida Chem. Co., Ltd. Na_2PdCl_4 (>98.0%) was purchased from Sigma Aldrich. Titanium tetraisopropoxide ($Ti(Oi\text{-}Pr)_4$) was obtained from Wako Pure Chem. Ind., Ltd. and FA (>98%) was purchased from Kanto Chem. Co., Inc. 1,5-pentanediol (>97%) was obtained from Tokyo Chem. Ind. Co., Ltd. All reagents were used without further purification.

2.2 Preparation of TiO_2 nanoparticles

Fig. 1 shows an experimental apparatus used for the MW heating (Shikoku Keisoku Kogyo K.K.; μ type, maximum output power 750 W). A three-necked glass flask was placed in the MW oven and a mixture of metallic reagent and surfactant was added into the flask. A reflex tube and a thermocouple were installed into a MW oven through holes in the top. A thermocouple made of an optical fiber, which is not damaged under MW irradiation, was used.

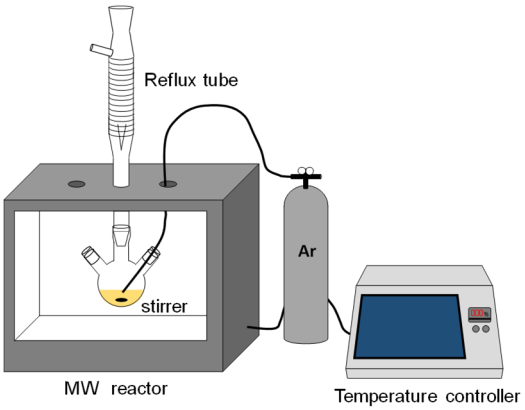

Fig. 1. Microwave reactor used for the preparation of Au@Pd/TiO_2 catalysts.

When TiO_2 nanoparticles were prepared by MW heating, 3 mmol $Ti(Oi\text{-}Pr)_4$ was added to 50 ml of 1,5-pentanediol.[16] The solution was irradiated in the MW oven at 200 W for 3 min. Then, 2 ml of distilled water was added to this solution and MW was irradiated again at 700 W for 1 h. The solution temperature increased to 175 °C after 3 min heating at 200 W. It dropped to 150 °C after injection of distilled water and increased again to about 195 °C after 6 min at 700 W and became nearly constant after that. For the use of TiO_2 as a support for metallic nanoparticles in the next step, products were obtained by centrifuging the colloidal solution at 15,000 rpm for 30 min two times. Then, they were redispersed in 50 ml of distilled water.

2.3 Preparation of bare Au@Pd nanocatalysts

Au@Pd core-shell nanoparticles were formed by using a two-step reduction method of metallic salts. First, Au core nanoparticles were formed by the following procedure. 45 ml of 2.22 mM $HAuCl_4{\cdot}4H_2O$ aqueous solution was heating at 100 °C under conventional oil-bath heating. Then, 5 ml of 100 mM sodium citrate aqueous solution was added, and the reagent solution was kept at 100 °C for 1 h. After that, 5 ml of 0.76 M PVP aqueous solution was added as a protecting agent. The product solution was centrifuged at 15,000 rpm for 100 min, and redispersed in distilled water. It was repeated two times and finally dispersed in 12.8 ml of distilled water.

In the second step, Au@Pd nanoparticles were prepared by MW heating of a mixture of 6.4 ml of Au core solution, 5 ml of 10 mM Na_2PdCl_4 aqueous solution, 5 ml of 0.38 M PVP aqueous solution, and 3.6 ml of distilled water. The reagent solution was heated by MW

irradiation at 400 W for 10 min under Ar gas bubbling. The Ar gas was used to suppress oxidation of Pd shell. The solution was centrifuged at 12,000 rpm for 100 min, and redispersed in ethanol. This procedure was repeated three times. Similar centrifugal separation was carried out three times in distilled water, and it was finally redispered in 10 ml of distilled water.

2.4 Preparation of Au@Pd/TiO2 nanocatalysts

After mixing 6.4 ml of Au core solution with 3.6 ml of TiO_2 solution involving 3.6 mmol TiO_2 molecules under ultrasonic irradiation for 3 h, 5 ml of 10 mM Na_2PdCl_4 and 10 ml of 0.79 M PVP aqueous solutions were added. Then, the reagent solution was heated by MW irradiation at 400 W for 10 min under Ar gas bubbling. The same centrifugal separation procedure as used the preparation of Au@Pd nanoparticles was used for the synthesis of 10 ml of aqueous Au@Pd/TiO_2 catalyst solution.

2.5 Characterization of product particles

For TEM and TEM-EDS (JEM-2100F; JEOL) observations, samples were prepared by dropping colloidal solutions of the products onto Cu grids. The average sizes of product particles were determined by measuring more than 100 particles in TEM images. The XPS spectra of the product were measured using Al Ka radiation (AXIS-165; Shimadzu Corp.).

2.6 Hydrogen generation activity of Au@Pd and Au@Pd//TiO2 nanocatalysts

Hydrogen production rate from decomposition of FA was measured using the apparatus shown in Fig. 2. The hydrogen production activity of the prepared samples was examined using the following method: the total gas volume from a stirred glass tube containing 20 ml of 0.25 M FA aqueous solution and the prepared sample (metallic catalyst weight of 5.8 mg) was measured using a gas burette.

The hydrogen gas volume produced per gram of Au@Pd and Au@Pd/TiO_2 catalysts per hour was calculated using Eq. (2).

$$HCOOH \rightarrow H_2 + CO_2 \quad (1)$$

$$R_{initial} = V_{gas}/(2\ m_{metal}\ t) \quad (2)$$

In this equation, $R_{initial}$ represents the initial rate of hydrogen generation when conversion x_a reaches 20%, V_{gas} is the volume of the initial

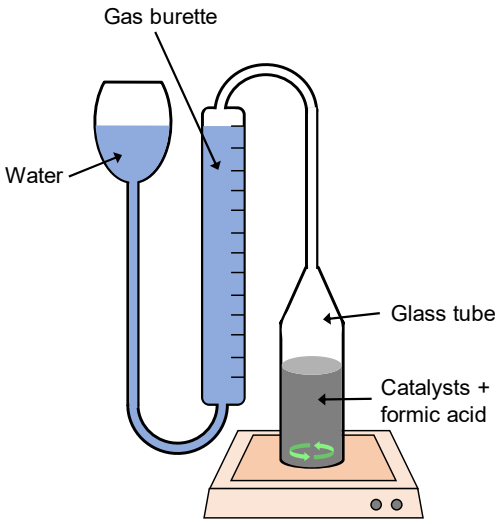

Fig. 2. Gas burette used for the hydrogen production from decomposition of formic acid using Au@Pd and Au@Pd/TiO_2 catalysts.

generated gas (H_2 + CO_2), when x_a reaches 20%, m_{metal} is the weight of the metallic catalyst, and t is the reaction time when x_a reaches 20%.

3. Results and discussion

3.1 TEM and TEM-EDS images of Au@Pd and Au@Pd/TiO2 catalysts

Figs. 3a and 3b show TEM image and XRD pattern of TiO_2 particles, respectively. Results show that TiO_2 support prepared by MW heating was solely anatase-type with an

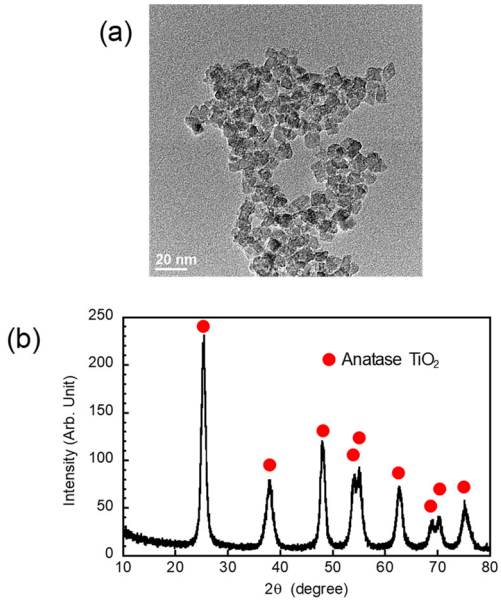

Fig. 3. (a) TEM image and (b) XRD pattern of TiO_2 prepared by MW heating.

average diameter of 10±2 nm. Fig. 4 shows a typical TEM image of Au particles prepared by oil-bath heating, where spherical nanoparticles with an average diameter of 10±2 nm are observed.

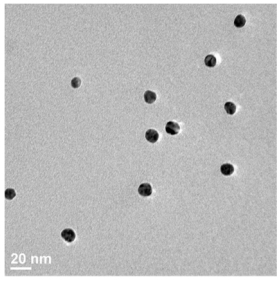

Fig. 4. TEM image of Au nanoparticles prepared by oil-bath heating.

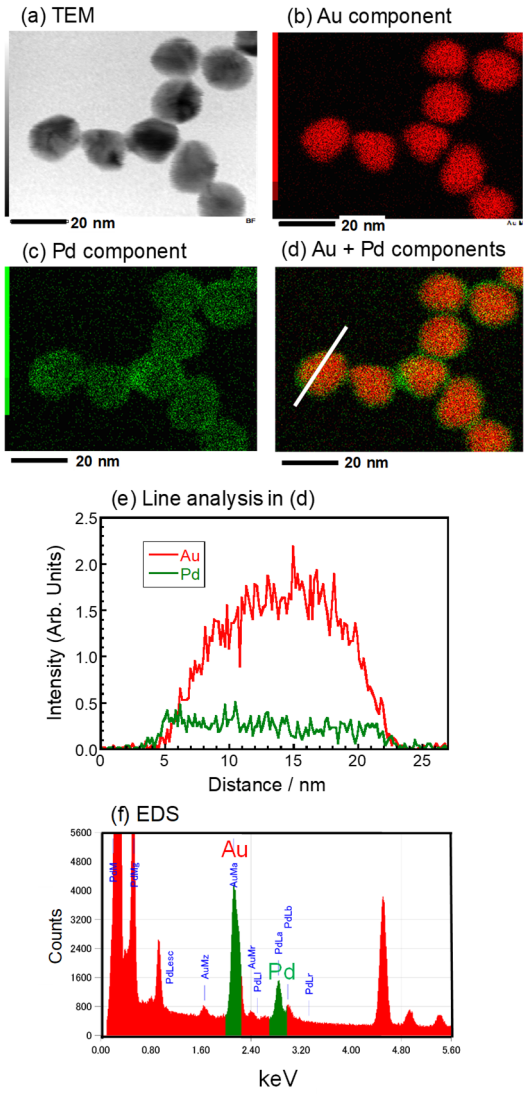

Fig. 5. (a)-(d) TEM and TEM-EDS images, (e) line analysis, and (f) EDS of Au@Pd nanoparticles.

Figs. 5 and 6 displays TEM and TEM–EDS data of Au@Pd and Au@Pd/TiO_2 catalysts prepared by MW heating, respectively. On the basis of these data, uniform Pd shells with an average thickness of 3±1 nm are formed on Au cores and Au@Pd catalysts with an average diameter of 15±2 nm were loaded uniformly on TiO_2 nanoparticles. The Au : Pd atomic ratio in Au@Pd catalysts was estimated to be about 7 : 3, respectively, from TEM-EDS data.

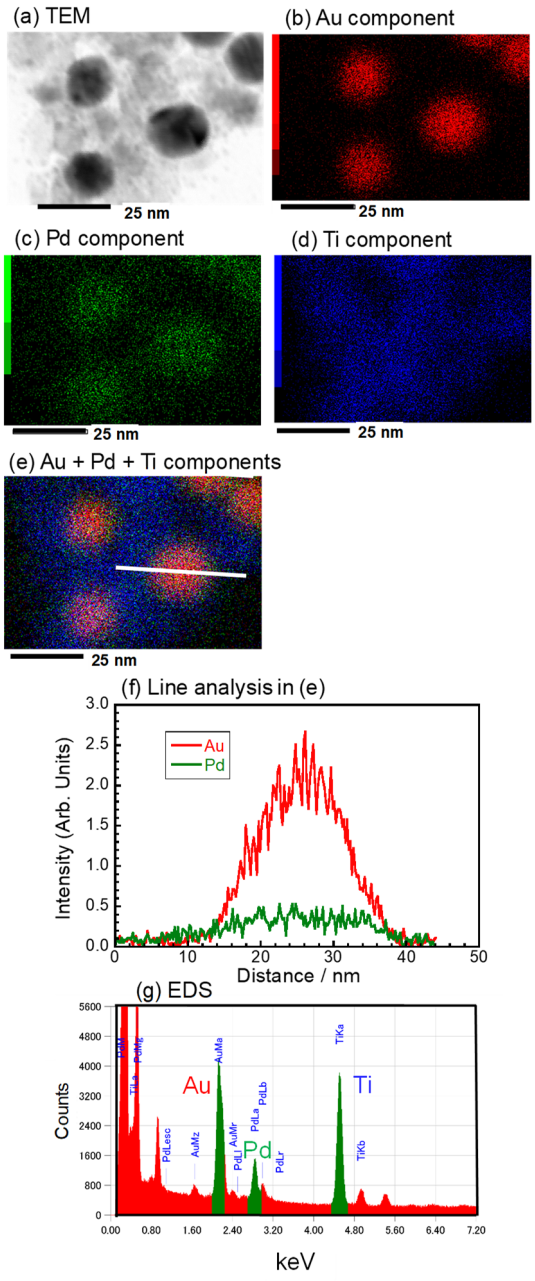

Fig. 6. (a)-(e) TEM and TEM-EDS images, (f) line analysis, and (g) EDS of Au@Pd/TiO_2 nanoparticles.

3.2 XPS spectra of Au@Pd and Au@Pd/TiO2 catalysts

To characterize chemical states of Au@Pd and Au@Pd/TiO_2 catalysts, XPS spectra were measured. In the range of 80–90 eV (Fig. 7a), Au $4f_{5/2}$ and $4f_{7/2}$ peaks are observed. The binding energies of the stronger $4f_{7/2}$ peaks are observed at 83.3 eV in both Au@Pd and Au@Pd/TiO_2 catalysts. These peaks shift to a lower value by 0.7 eV compared to that of pure Au ($4f_{7/2}$ = 84.0 eV), as shown by a red dotted lines.[17] Negative shifts of Au peaks in Au@Pd and Au@Pd/TiO_2 indicate that the electron density around Au atom increases and the binding energy decreases in comparison with that of pure Au atoms due to an effect of the presence of Pd shell. Similar negative chemical shifts in Au@Pd and Au@Pd/TiO_2 indicates that the presence of TiO_2 catalytic support does not affect the electronegativity of Au core.

In the range of 330–345 eV (Fig. 7b), Pd $3d_{3/2}$ and $3d_{5/2}$ peaks are observed. No peaks of PdO are found indicating that oxidation of Pd shell is insignificant. The Pd $3d_{3/2}$ and $3d_{5/2}$ peaks in Au@Pd/TiO_2 are much sharper than those in Au@Pd, indicating that energy distributions of Pd states in Au@Pd/TiO_2 are narrower than those in Au@Pd. The binding energy of the stronger Pd $3d_{5/2}$ peak in Au@Pd shifts to a lower value of 335.1 eV by 0.2 eV, whereas that in Au@Pd/TiO_2 shifts to a further lower value of 334.5 eV by 0.8 eV compared to that of pure Pd ($3d_{5/2}$ = 335.3 eV), as shown by a red dotted line.[17] It is known that work functions of Au (5.1 eV)[18] and Pd (5.1 eV) are identical, and they are larger than that of anatase-TiO_2 (4.0 eV). Therefore, the larger negative shift of Pd peak in Au@Pd/TiO_2 than that of Au@Pd is explained by electron transfer from TiO_2 to Pd shells in Au@Pd/TiO_2 particles.

3.3 Initial H_2 production rates from formic acid decomposition using Au@Pd and Au@Pd/TiO_2 catalysts

The initial H_2 production rates ($R_{initial}$) of Au@Pd and Au@Pd/TiO_2 catalysts from FA decomposition were measured using a gas burette (see Fig. 2). Detailed gas analyses for CO_2, H_2, and CO were performed on a gas chromatograph and no CO emission was detected using GC for all samples at 30–90 °C. This implies that the following decomposition channel is negligible in our conditions.

$$HCOOH \rightarrow CO + H_2O \qquad (3)$$

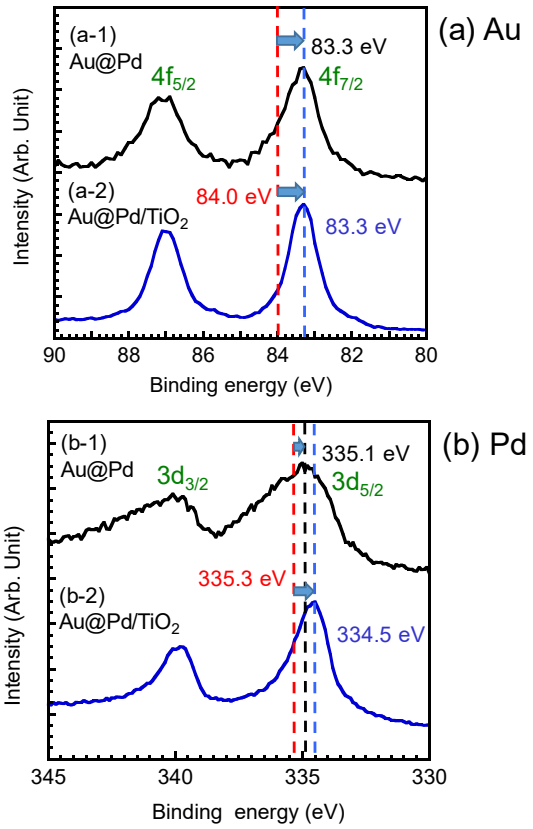

Fig. 7. XPS spectra of (a) Au and (b) Pd components of Au@Pd and Au@Pd/TiO_2 nanocatalysts. Standard peak positions are shown by dotted red lines.

Temporal variation of total gas (H_2 + CO_2) generation by decomposition of FA using Au@Pd and Au@Pd/TiO_2 catalysts at 30, 60, and 90 °C was measured (Fig. 8). With increasing the reaction temperature from 30 °C to 90 °C, the formation rate of H_2 + CO_2 gases increases. The formation rate of H_2 + CO_2 gases using Au@Pd/TiO_2 catalysts is faster than that using bare Au@Pd in all the three temperatures, although difference in the catalytic activity decreases with increasing the reaction temperature.

Table 1 shows the $R_{initial}$ values obtained from equation (2) along with reported data for Ag@Pd, $Ag_{82}Pd_{18}$@Pd, and $Ag_{93}Pd_7$@Pd/TiO_2 catalysts.[9,11] With increasing the reaction temperature from 30 °C to 90 °C, the $R_{initial}$ values of Au@Pd and Au@Pd/TiO_2 catalysts increase by factors of 49 and 25, respectively. The $R_{initial}$ values of Au@Pd/TiO_2 are larger than those of Au@Pd by factors of 1.5–3.0. The $R_{initial}$ values of Au@Pd and Au@Pd/TiO_2 are smaller than those of $Ag_{82}Pd_{18}$@Pd and $Ag_{93}Pd_7$@Pd/TiO_2 by factors of 1.6–17 and

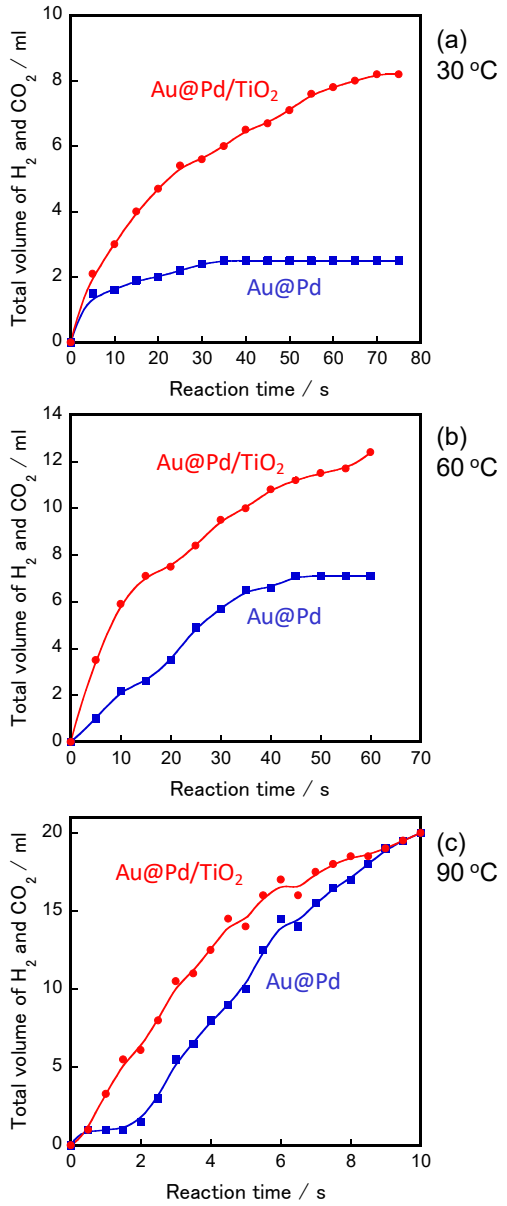

Fig. 8. Gas generation by decomposition of formic acid (0.25 M, 20 ml) versus time in the presence of Au@Pd and Au@Pd/TiO_2 catalysts at (a) 30 °C, (b) 60 °C, and (c) 90 °C.

Table 1. Initial hydrogen production rates from catalytic decomposition of formic acid in water.

Catalyst	Temperature (°C)	$R_{initial}$ (L / g h)	Refs
Au@Pd	30	0.043	This work
Au@Pd	60	0.12	This work
Au@Pd	90	2.1	This work
Au@Pd/TiO_2	30	0.13	This work
Au@Pd/TiO_2	60	0.21	This work
Au@Pd/TiO_2	90	3.2	This work
Ag@Pd	20	3.67	Ref. 9
Ag@Pd	35	4.58	Ref. 9
$Ag_{82}Pd_{18}$@Pd	27	0.71 ± 0.06	Ref. 9
$Ag_{82}Pd_{18}$@Pd	60	1.98 ± 0.18	Ref. 9
$Ag_{82}Pd_{18}$@Pd	90	3.34 ± 0.22	Ref. 9
$Ag_{93}Pd_7$@Pd /TiO_2	27	46.03 ± 2.27	Ref. 11
$Ag_{93}Pd_7$@Pd /TiO_2	60	143.77 ± 3.33	Ref. 11
$Ag_{93}Pd_7$@Pd /TiO_2	90	371.21 ± 10.54	Ref. 11

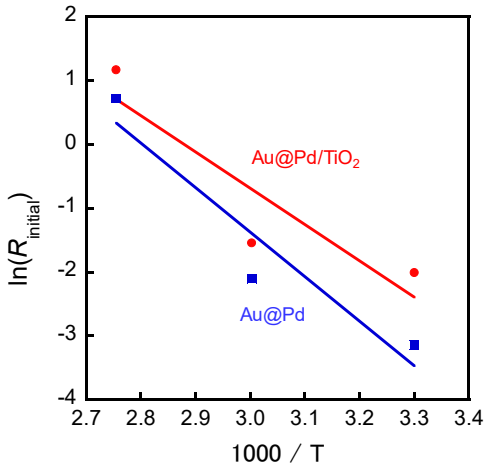

Fig. 9. Plots of ln($R_{initial}$) vs 1000/T for Au@Pd and Au@Pd/TiO_2 catalysts.

116–685, respectively. These results indicate that Au core is less active than AgPd alloy core in M@Pd (M = metal or alloy) core-shell catalysts.

The apparent activation energies were estimated from the following relation using $R_{initial}$ data given in Table 1.

$$\ln(R_{initial}) = -E_a/RT + C \qquad (4)$$

In this equation, E_a is the apparent activation energy, and C is a constant. Fig. 9 shows plots of ln($R_{initial}$) vs 1000/T for Au@Pd and Au@Pd/TiO_2 catalysts. From slopes of each line, the E_a values were estimated as 58 and 47 kJ mol^{-1} for Au@Pd and Au@Pd/TiO_2, respectively. The lower E_a value obtained using Au@Pd/TiO_2 than that using Au@Pd agrees with the higher catalytic activity of the former catalyst.

The work function has been regarded as an important parameter of the catalytic system for the FA decomposition system over M@Pd (M = Ag, Rh, Au, Ru, Pt) core–shell catalysts. The catalytic activity increases concomitantly with

decrease in the work function.[9] The current results show that the hydrogen production rate is greatly enhanced in the presence of TiO_2 for the Au@Pd system, as observed for AgPd@Pd catalyst.[10-13] Larger negative chemical shift (0.8 eV) was observed for the XPS peak of Pd ($3d_{5/2}$) shell for Au@Pd/TiO_2 compared with that for Au@Pd (0.2 eV), because the work function of TiO_2 (4.0 eV) is lower than Pd (5.1 eV) and Au (5.1 eV). This implies that electrons are transferred from TiO_2 to Pd shells in the presence of TiO_2. Such electron transfer from the TiO_2 support to Pd shells causes the higher catalytic activity of Au@Pd/TiO_2 than that of Au@Pd. When the negative peak shift of Pd ($3d_{5/2}$) in Au@Pd/TiO_2 (0.8 eV) was compared with that of AgPd@Pd/TiO_2 (2 eV)[11], it is smaller by 1.2 eV. This indicates that a smaller amount of electrons is transferred from TiO_2 to Pd shells in Au@Pd/TiO_2 catalyst. This is a main reason why the catalytic activity of Au@Pd/TiO_2 is lower than that of AgPd@Pd/TiO_2.

The current results show that the apparent activation energy of reaction (1) using Au@Pd/TiO_2 catalyst decreases by 19% in the presence of TiO_2. Based on previous density functional theory calculations on intermediate species,[19,20] formate is an important intermediate in FA decomposition on metallic catalysts. A possible decomposition scheme of formate on Au@Pd/TiO_2 is shown in Fig. 10. Decomposition starts by activating the C–H bond of formate adsorbed on the catalytic surface. Under our conditions, monodentate formate (species A) transforms efficiently to more stable bidentate formate (species B), in which both oxygen atoms bind to the catalyst surface. Otherwise CO is formed through decomposition of monodentate formate (species A).[9] Bidentate formate (species B) decomposes into CO_2* + H* (species C), where X* denotes intermediates adsorbed onto the surface. Recombination of two H* and CO_2* leaving from the surface results in the formation of CO_2 + H_2 gases (species D). Based on theoretical calculations on potential energy surfaces (PESs) of the FA decomposition reaction, the energy barrier from species B to species C is highest. It is the rate-determining step. The greater degree of electron transfer from the Pd layer to intermediate species A–C in the presence of TiO_2 strengthens the adsorption of formates and decreases the energy barriers of hydrogen formation and proton diffusion over catalysts.

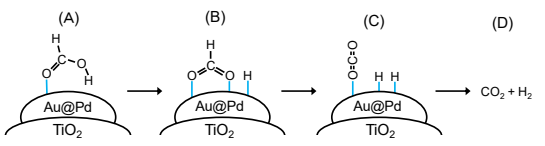

Fig. 10. The schematic diagram of formic acid decomposition pathways on the Pd surface of Au@Pd/TiO_2.

4. Summary and Conclusion

Using an MW-heating method, TiO_2-supported Au@Pd core–shell nanoparticles with an average diameter of 15±2 nm were prepared. To examine the effects of TiO_2, bare Au@Pd were synthesized under MW heating in the absence of TiO_2. The initial hydrogen formation rate of Au@Pd/TiO_2 from FA, 0.13 L g^{-1} h^{-1}, was 3.0 times higher than that of bare Au@Pd at 30 °C. The apparent activation energy of dehydrogenation of FA by Au@Pd catalysts decreased from 58 kJ mol^{-1} to 47 kJ mol^{-1} in the presence of the TiO_2 support. When XPS spectra of the catalysts were observed, larger negative chemical shifts were observed for Pd peaks of Au@Pd/TiO_2 in comparison with those of bare Au@Pd because of electron-donating effects of TiO_2 to Pd shells. Based on the findings presented above, the marked enhancement of catalytic activity of Au@Pd/TiO_2 was attributed to electron transfer from TiO_2 to Au@Pd catalysts, promoting C–H cleavage of FA over the surface of Au@Pd/TiO_2 nanocatalysts (species B → C in Fig. 10). In fact, CO emission, which reduces catalytic activity of Au@Pd/TiO_2, was not observed through decomposition of monodentate formate (species A in Fig. 10) at 30–90 °C.

Acknowledgments

This work was supported by JSPS KAKENHI Grant number 25286003.

References

1) X. C. Zhou, Y. Huang, W. Xing, C. Liu, J. Liao, and T. Lu, *Chem. Commun.*, 3540 (2008).
2) Y. Huang, X. Zhou, M. Yin, C. Liu, and W. Xing, *Chem. Mater.*, 22, 5122 (2010).
3) M. Navlani-García, K. Mori, M. Wen, Y. Kuwahara, and H. Yamashita, *Bull. Chem. Soc. Jpn.*, 88, 1500 (2015).
4) C. Hu, J. K. Pulleri, S-W Ting, and K-Y. Chan, *Int. J. Hydrogen Energy*, 39, 381 (2014).
5) X. Wang, G.-W. Qi, C.-H. Tan, Y.-P. Li, J. Guo, X.-J. Pang, and S.-Y. Zhang *Int. J. Hydrogen Energy*, 39, 837 (2014).

6) S. Zhang, O. Metin, D. Su, and S. Sun, *Angew. Chem., Int. Ed.*, 52, 3681 (2013).
7) Y. Jiang, X. Fan, M. Chen, X. Xiao, Y. Zhang, C. Wang, and L. Chen, *J. Phys. Chem. C*, 122, 9, 4792 (2018).
8) M. Navlani-García, D. Salinas-Torres, and D. Cazorla-Amorós, *Energies*, 12, 4027 (2019).
9) K. Tedsree, T. Li, S. Jones, C. W. A. Chan, K. M. K. Yu, P. A. J. Bagot, E. A. Marquis, G. D. W. Smith, and S. C. E. Tsang, *Nat. Nanotechnol.*, 6, 302 (2011).
10) M. Hattori, H. Einaga, T. Daio, and M. Tsuji, *J. Mater. Chem. A*, 3, 4453 (2015).
11) M. Hattori, D. Shimamoto, H. Ago, and M. Tsuji, *J. Mater. Chem. A*, 3, 10666 (2015).
12) M. Tsuji, D. Shimamoto, K. Uto, M. Hattori, and H. Ago, *J. Mater. Chem. A*, 4, 14649 (2016).
13) M. Tsuji, D. Shimamoto, and M. Hattori, *Chimica Oggi*, 34, 55 (2016).
14) M. Tsuji, M. Hashimoto, Y. Nishizawa, M. Kubokawa, and T. Tsuji, *Chem, Eur. J.*, 11, 440 (2005).
15) K. M. Koczkur, S. Mourdikoudis, L. Polavarapu, and S. E. Skrabalak, *Dalton Trans.*, 44, 17883 (2015).
16) T. Yamamoto, Y. Wada, H. Yin, T. Sakata, H. Mori, and S. Yanagida, *Chem. Lett.*, 38, 964 (2011).
17) XPS (X-ray Photoelectron Spectroscopy) Database, XPS Spectra -Peak Position | Binding Energy-, http://techdb.podzone.net/eindex.html.
18) H. B. Michaelson, *J. Appl. Phys.*, 48, 4729 (1977).
19) A. Vittadini, A. Selloni, F. P. Rotzinger, and M. Gratzel, *J. Phys. Chem. B*, 104, 1300 (2000).
20) C. Hu, S.-W. Ting, K.-Y. Chan, and W. Huang, *Int. J. Hydrogen Energy*, 37, 15956 (2012).